JJEE
Volume 3, Number 2, 2017
Pages 126-137
Jordan Journal of Electrical Engineering
ISSN (Print): 2409-9600, ISSN (Online): 2409-9619

Reduced Cell Size Metamaterial Based Wideband Infrared Absorber

Hamzeh M. Jaradat

Department of Telecommunications Engineering, Yarmouk University, Irbid, Jordan
e-mail: Hamzehjaradat@yu.edu.jo

Received: March 8, 2017 *Accepted: April 27, 2017*

Abstract— A novel design of metamaterial (MTM) based absorber with reduced cell size is proposed in this paper. The absorber is designed to operate in the mid infrared (IR) regime using gold nano-pillar inclusions embedded in a dielectric spacer. The absorption band can be controlled by adjusting the nano-pillar's properties. Numerical simulations have been conducted to investigate the effect of these inclusions on the absorber performance. Moreover, a wideband absorber is designed by combining four different sized resonant elements within the unit cell. The absorber shows enhanced characteristics such as large bandwidth, small cell size to wavelength ratio and high absorption level for wide range of incident angles for different wave polarizations. The achieved bandwidth is around 60% with normalized absorption percentage of 80% over the band 5.2-9.8μm, and cell size ratio of 0.34λ.

Keywords— Metamaterials, Multi-sized absorber, Nano-pillar inclusions, Subwavelength structures, Wideband IR absorber.

I. INTRODUCTION

Metamaterial based devices have been gaining much attention during the past decade. This is due to their unique and unusual characteristics such as compact size, high efficiency, and suitability for various applications. The significance of metamaterials arises from the ability to manipulate and control their properties at any desired frequency band. This is usually done by appropriately designing subwavelength resonant elements that collectively interact with the electromagnetic (EM) waves. The nature of electric and magnetic interactions determines electric and magnetic properties. Lately, research has focused on a unique type of MTM based devices that can absorb the ambient EM radiation. This type is called perfect absorber. It has been designed to possess single [1], dual [2], multiple [3], [4], or wide band absorption characteristics [5] depending on the application required at such frequency range as microwave [6], terahertz (THz) [7] and optical regimes [8]. Microwave absorbers are used to suppress the undesired radiation. Terahertz and optical absorbers are commonly used in thermal imaging, explosive detection, bolometers [9], solar cells [10], IR spectroscopy [11], and light harvesting. Because of the great importance of these structures, particularly at IR and optical wavelengths, several efforts have been conducted to improve and enhance absorption characteristics such as absorption strength, bandwidth, and polarization independency. Large bandwidths are significantly desired in solar cells and light harvesting applications. Therefore, several methods were introduced in literature to enhance the bandwidth. The basic principle is to produce multiple adjacent resonances within the band of interest to form one continuous broad band. This is commonly done by overlaying multiple layers [12], [13], using a planar multi-sized resonant pattern [14], or combining both strategies [15]. Even though large bandwidth could be achieved, multi-layer absorbers are difficult to fabricate because they require precise alignment, and are relatively thick. On the other hand, the absorbers based on multi-sized elements are very thin structures, and easy to implement. They suffer from low absorption efficiency due to the limited number of elements that can fit within the unit cell. Increasing the number of elements needs a larger unit cell, which increases the ratio of unit cell size to wavelength. It has been verified that the large cell

Corresponding author's e-mail: Hamzehjaradat@yu.edu.jo

size compared to the operating wavelength reduces the efficiency caused by scattering effect [16]-[18]. Scattering problem is more apparent when the cell size becomes comparable to the wavelength, especially for wideband structures. Consequently, resonances at shorter wavelengths would exhibit more scattering contribution that degrades the absorption efficiency [6], [19], [20].

In this work, the design of MTM based absorber exhibiting improved absorption characteristics is introduced and analyzed. The cell size is reduced compared to conventional absorbers at the same operating wavelength. This is advantageous in reducing the scattering effect and enhancing the absorption efficiency. The proposed structure utilizes an array of nano pillar inclusions that has a direct impact on shifting the resonances to longer wavelengths. These inclusions are also exploited to construct a wideband absorber using multi-sized element technique. The absorption bandwidth is extended using four different circular discs. Small cell size, large bandwidth and high absorption level are the main characteristics of the proposed design.

This paper is organized as follows; section II reviews the design of a single band MTM absorber based on conductive circular discs pattern. Section III discusses geometry, simulation process and results of the proposed absorber structure. Section IV demonstrates the significance of the proposed design by constructing a wideband absorber with enhanced characteristics. Finally, main conclusions are summarized in section V.

II. CONVENTIONAL METAMATERIAL BASED ABSORBER

The traditional approach in designing most of the MTM based absorbers is to stack three different layers over each other in the following manner: conductor, dielectric, conductor. In optical and IR regimes, conductive layers are commonly made of noble metals such as gold (Au) and silver (Ag). This is because the incident wave strongly interacts with the free electrons within the metal surface creating surface plasmon resonance (SPR) [21]. These electrons start to oscillate along the metal-dielectric interface and collectively coincide with the electric field of the incident light.

In order to point out the significance of this work, the characteristics of the previously reported absorber are studied [22], [26]. This structure has been extensively investigated and reported in literature due to its simplicity, which can be scaled easily and utilized at different frequency bands. Fig. 1a shows the geometry of one unit cell of a single band IR absorber. The top layer is composed of periodic conductive patterns of resonant circular gold discs of radius $R_1 = 450\text{nm}$ and height of 70nm. Silicon nitride (S_3N_4) dielectric spacer occupies the middle layer of thickness $\text{d} = 100\text{nm}$. It is assumed to be lossless with a dielectric constant of $\varepsilon_\text{r} = 4.4$. It is widely used in optical applications since it possesses a low surface roughness that limits scattering losses.

The bottom layer is made of thin gold film of thickness t_g. It serves like a ground mirror that reflects the incident wave all back. The film thickness has to be larger than the skin depth to make sure that the incident wave cannot penetrate through this layer. Therefore, t_g is chosen to be $200nm$, which is enough to achieve zero transmission and complete reflection. The period size along the *x*-direction is $a_x = 1.73\mu m$ and along the y-direction is $a_y = 2.06\mu m$. The structure dimensions used for this design are chosen so that results can be properly compared with the proposed design results [26]. The disc radius determines the resonance frequency as reported in [26]. The other structure parameters are optimized to produce the best result.

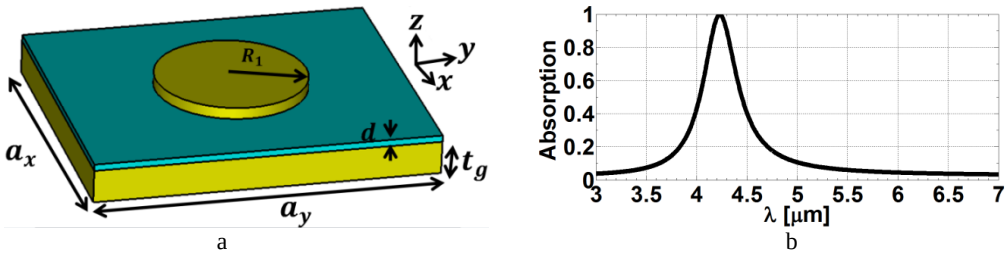

a b

Fig. 1. Conventional MTM based absorber: a) unit cell geometry and, b) absorption response

The numerical results are obtained using the commercial full wave simulation package microwave studio computer simulation tool (MWS CST) [23]. The software has a build-in template for simulating periodic planar structures. The frequency domain solver is utilized with unit cell boundaries set along *x* and *y* directions. This setup ensures that infinite periodicity is considered for simulation in the *x*-*y* plane. Two open floquet ports are placed above and below the structure. The incident wave signal is excited from the input port, which is placed at a distance over the structure. The incident wave is propagating along the negative *z*-direction. Drude dispersion model for gold dielectric function is considered in the simulation [24], which is given by (1):

$$\varepsilon(\omega) = 1 - \frac{\omega_p^2}{\omega^2 + i\gamma\omega} \tag{1}$$

where, ω_p is the plasma frequency; and γ is the collision frequency. The experimental fitted values have the following values: $\omega_p = 2\pi \times 2184 \times 10^{12}$ rad/s, and $\gamma = 2\pi \times 6.45 \times 10^{12}$ rad/s. The absorbed power can be calculated from the scattering parameters using (2):

$$A(\omega) = 1 - |S_{11}(\omega)|^2 - |S_{21}(\omega)|^2 - D(\omega) \tag{2}$$

where, $A(\omega)$ is the normalized absorbed power; $|S_{11}(\omega)|^2$ is the reflected power; $|S_{21}(\omega)|^2$ is the transmitted power; and $D(\omega)$ is the scattered power. The transmitted power is zero because of the ground film. The simulated absorbed power is depicted in Fig. 1b, which shows that a perfect absorption peak occurs at wavelength $\lambda = 4.5\mu m$. Since the dielectric spacer is lossless, most of the absorbed power gets dissipated as ohmic loss through conductors. The scattered power is negligible since the period size is relatively small compared to the operating wavelength, which is nearly 0.45λ.

The resonance wavelength can be controlled by either tuning the disc radius or the spacer dielectric constant. The period size and the spacer thickness have no effect on the resonance wavelength, but they influence the absorption level. Scaling the resonance wavelength to any desired wavelength requires readjusting all structure parameters. For example, Fig. 2 shows a 2D absorption strength versus spacer thickness in the range $3 - 7\mu m$. Absorption starts to weaken drastically when spacer thickness d is larger than $0.15\mu m$. The resonance wavelength is almost unaffected.

A comprehensive parametric study is already investigated in [18], [26], [27] which addresses the effect of each parameter on the absorption strength and resonance wavelength. In the following section, an additional degree of freedom to control the absorption band will be discussed in details.

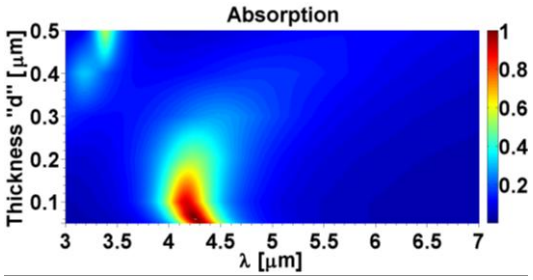

Fig. 2. 2D absorption strength plot for various spacer thickness "***d***"

III. THE PROPOSED DESIGN OF COMPACT SIZE ABSORBER

A. Absorber Design Utilizing Gold Nano-Pillar Inclusions

Indeed, controlling the absorbed resonance is preferable in the absorber design. The resonance wavelength should be controlled independently and tuned to any desired band. This is done by properly scaling the structure's dimensions. By introducing cylindrical gold nano-pillar inclusions [25] within the dielectric spacer, it could be possible to control the absorption band without varying the cell size, spacer material or conductive pattern size. Fig. 3a shows the modified absorber structure unit cell, which comprises from the following layers arranged from bottom to top: gold ground mirror, cylindrical gold nano-pillar array embedded in the dielectric spacer and gold circular disc. The nano-pillars array is $N \times N$ elements, each of which has radius "R", height "T", and is separated by "S_x", "S_y" in the x and y directions, respectively. The rest of the parameters are already defined in the previous section.

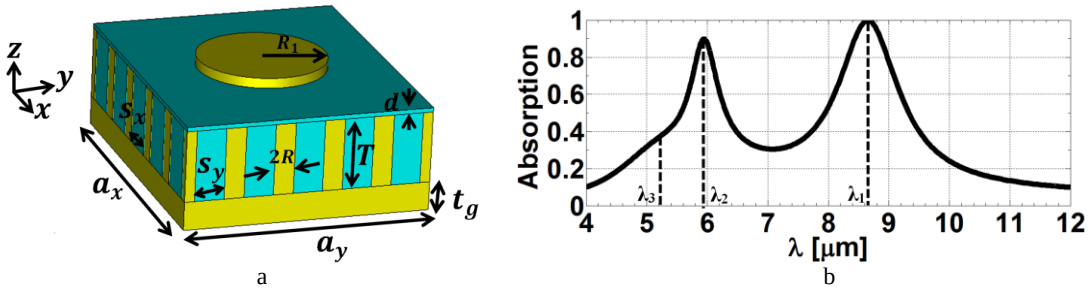

a b

Fig. 3. The proposed MTM based absorber: a) unit cell geometry and, b) absorption response

The structure dimensions are listed in Table 1. The corresponding absorption curve is depicted in Fig. 3b. Clearly there are two strong absorption bands centered at $\lambda_1 = 8.7\mu m$, $\lambda_2 = 5.95\mu m$ and one weak resonance at $\lambda_3 = 5.2\mu m$. The cell size to wave length ratio at each resonance is $0.23\lambda_1$, $0.34\lambda_2$ and $0.39\lambda_3$ for the first, second, and third resonance, respectively. An evident improvement is observed compared to the conventional MTM absorber discussed in section II. The achieved cell size to the operating wavelength ratio was around 0.45λ for the same disc radius and cell size.

TABLE 1
STRUCTURE DIMENSIONS FOR THE PROPOSED ABSORBER OF FIG. 3A

R_1	a_x	a_y	d	t_g	S_x	S_y	T	R	ε_r
$0.45\mu m$	$2.06\mu m$	$1.73\mu m$	$30nm$	$0.2\mu m$	$0.27\mu m$	$0.2\mu m$	$0.5\mu m$	$70nm$	4.41

B. Discussion and Analysis

In order to understand the absorption nature of each resonance, the distributions of fields are examined. The incident wave has a *y*-polarized electric field component (E_y) and *x*-magnetic field component (H_x). Due to the interaction between E_y and the disc surface charge, opposite charge polarities start to accumulate on the disc's surface. Fig. 4a shows the electric field vector at first resonance λ_1 for the yz cut plane. The left hand side of the disc has a negative charge, whereas the right hand side has a positive charge. The pillars near each side are charged with an opposite polarity charge. Therefore, a strong electric dipole moment is vertically formed between the disc surface and nano-pillar surfaces. This can be seen from the electric field enhancement in the region between the disc surface and pillars. Magnetic resonance is also observed, where the strong magnetic field is circulating around the disc. The xy cut plane shown in Fig. 4b indicates that the magnetic field component of the incident wave couples around the disc and induces a conductive circular current. The cut plane shows only the magnetic field in the dielectric spacer region. The field in the free space region is not shown. The current density field map is shown in Fig. 4c. It shows that a circulating current is driven through the disc and pillars, which are directly underneath the disc in the path indicated by the black arrow. The antiparallel currents are formed on the disc, ground film, and neighboring pillars. Therefore, all the incident power is dissipated in the conductors in the form of ohmic loss.

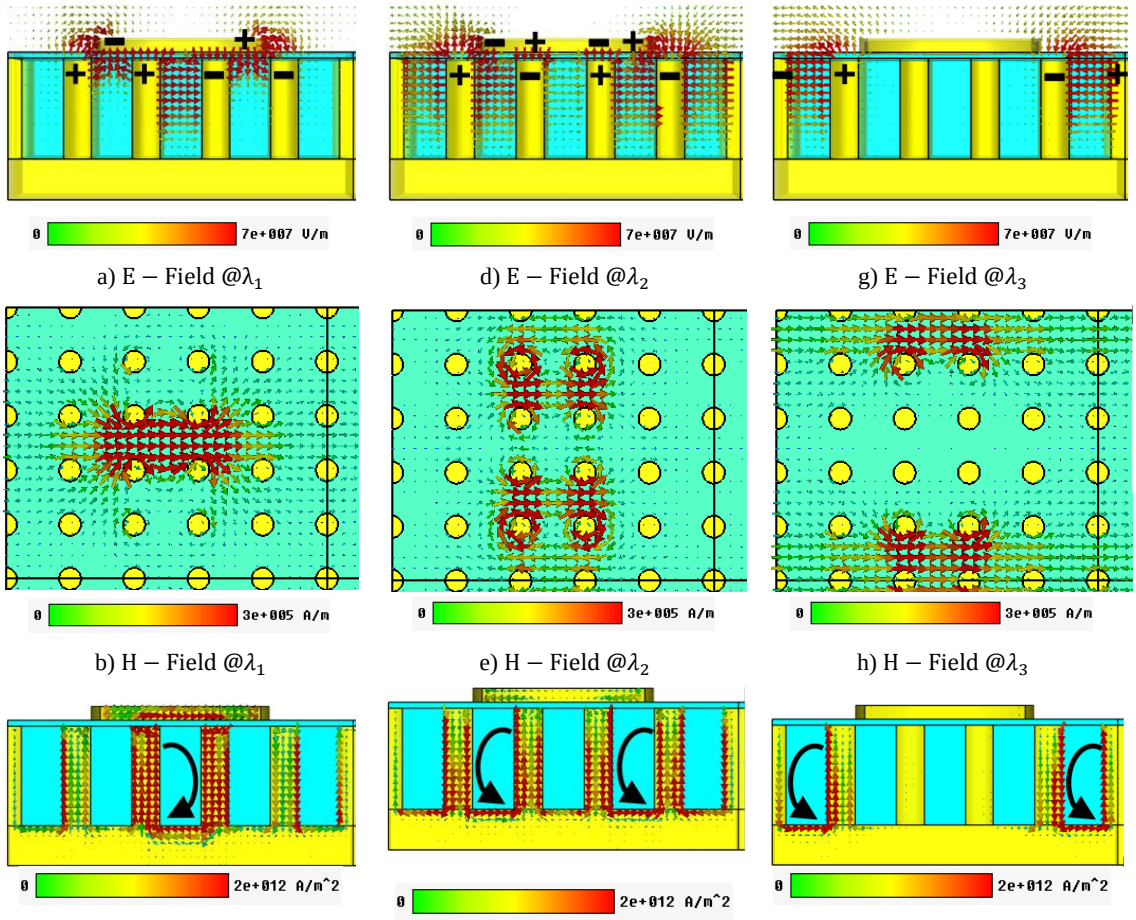

a) E − Field @λ_1 d) E − Field @λ_2 g) E − Field @λ_3

b) H − Field @λ_1 e) H − Field @λ_2 h) H − Field @λ_3

c) Current density @λ_1 f) Current density @λ_2 i) Current density @λ_3

Fig. 4. Electric, magnetic, and current density field maps at each resonance

The second resonance at λ_2 is attributed to a second order higher resonance mode. This is clearly observed from the electric field map depicted in Fig. 4d. The vector field shows that electric quadrupoles are formed between the disc and adjacent pillars for each side of the disc. The plus and minus signs indicate the polarity of charges on the disc surface and pillars' surfaces. The coupled magnetic field circulates around the pillars and induces circulating antiparallel currents as shown in Fig. 4e and 4f respectively. In contrast to the first two resonances, the third resonance "λ_3" does not depend on the disc size. It is only based on the interaction between the pillars located close to the edge of the unit cell. The electric dipole is formed between pillars on the side of the unit cell as indicated in Fig. 4g. The magnetic field in Fig. 4h drives the circulating antiparallel currents in the direction specified by the arrow in Fig. 4i. This resonance occurs in a close proximity to the second resonance "λ_2", but it is much weaker because of the large spacing between pillars.

C. Parametric Study

Introducing the nano-pillar inclusions in the spacer adds extra parameters that might have great impact on the absorption performance. To investigate this effect, several parametric studies have been conducted. Fig. 5a shows the absorption strength map with respect to the variation of pillar's height in the range 4-12μm. Red shift is observed when the height "T" increases. It is seen from the field maps that the two absorption bands depend strongly on the incident field interaction with the pillars. Thus, as the height goes larger, the resonance occurs at longer wavelength. Furthermore, pillar's radius "R" variation shown in Fig. 5b reveals that by increasing the radius, the first resonance "λ_1" shifts up in wavelength; and the absorption strength weakens. This is due to the increase of the effective dielectric constant underneath the disc. Also, it is observed that the surface under the disc becomes more conductive. This is because the top surfaces of the pillars occupy most of the surface area, which acts like a ground plane. Therefore, the effective thickness of the spacer approaches to the thickness "d". On the other hand, the second resonance at "λ_2" is slightly affected as can be seen from Fig. 5b. Very small red shift is observed when the radius increases. The third resonance "λ_3" starts to appear more prominent when the radius becomes larger. The absorption strength is enhanced due to decrease in spacing between the pillars, which yield to a stronger resonance.

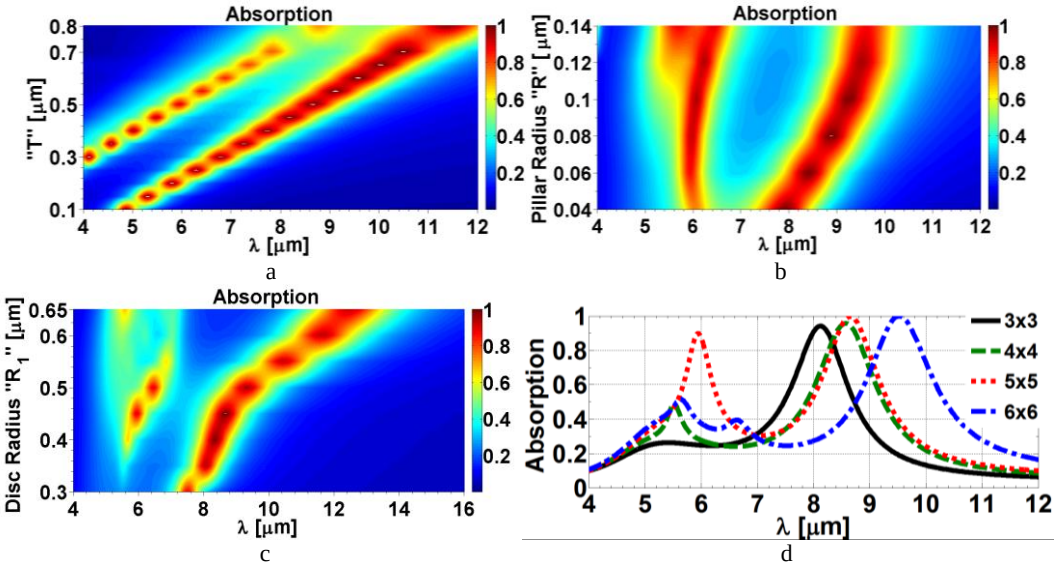

Fig. 5. Absorption response for various parameters: a) pillar's height "T", b) pillar's radius "R", c) disc radius "R_1", and d) number of pillars per unit cell

The circular disc radius "R_1" is swept between 0.3μm and 0.65μm with absorption response shown in Fig. 5c. As expected, bigger radius produces resonance at longer wavelength. The shift is observed for the resonances at "λ_1" and "λ_2". The third resonance at "λ_3" does not change, but it gets stronger at larger disc radius when the disc starts to interact with pillars at both sides of the unit cells. The same observations are applied when the number of pillars within the unit cell increases as depicted in Fig. 5d. From these curves, it is seen that resonances at "λ_1" and "λ_2" suffer red shift by increasing the number of pillars, while the third resonance is fixed.

So far, the single band absorber design with a controllable band has been discussed and analyzed. Based on the results obtained, the next section discusses, in details, the design of wideband absorber based on the gold nano-pillar inclusions by utilizing multi-sized elements.

IV. WIDEBAND ABSORBER BASED ON MULTI-SIZED DISCS

A. Structure Geometry and Simulation Results

In the previous section, the unit cell size is reduced by introducing nano-pillar inclusions. Therefore, absorbers with small cell size to wavelength ratio can be designed to reduce the scattering effect. Utilizing this result, the absorption band can be extended using multi-sized elements. The wideband absorber unit cell structure is illustrated in Fig. 6a. It consists of four circular discs, each of which has a different radius labeled as shown in the structure geometry. The radii of these discs are $R_1 = 0.45\mu m$, $R_2 = 0.38\mu m$, $R_3 = 0.35\mu m$, and $R_4 = 0.31\mu m$ for Disc1, Disc2, Disc3 and Disc4, respectively. The dimensions for the other structure parameters are listed in Table 1, which they are the same dimensions used for the structure in the previous section. The discs radii are chosen to produce multiple adjacent resonances as shown in Fig. 6b, where the colored curves represent the isolated absorption response for each disc. The combined response for all resonances forms a broad absorption band as represented by the black solid line. The absorption strength is better than 80% in the range 5.5-9.2 μm with full width half maximum bandwidth (FWHM) of 60%. The largest cell size to wavelength ratio is almost 0.34λ.

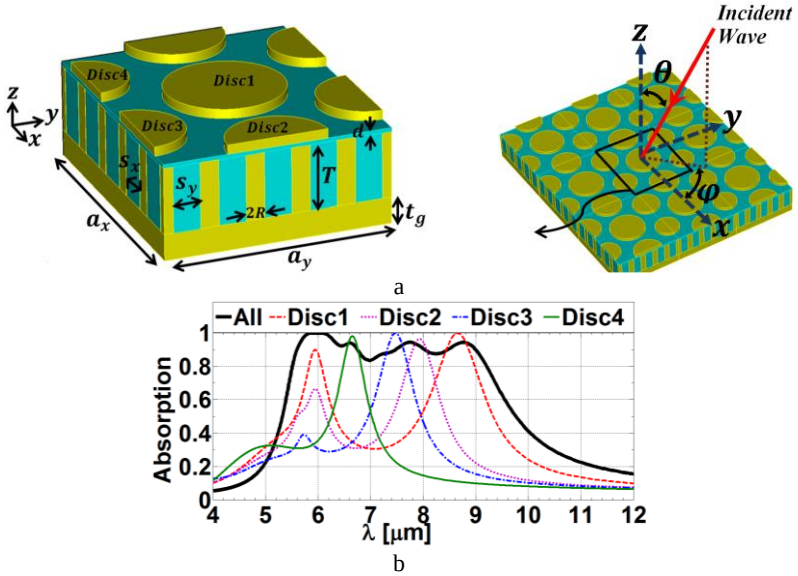

Fig. 6. Wideband absorber structure: a) unit cell, b) its absorption response with individual response for each disc

The performance of the proposed absorber is compared with the same structure but without using nano-pillar inclusions. The absorber, with only dielectric spacer, is simulated with all

dimensions fixed to the same dimensions listed in Table 1. The dielectric spacer thickness is optimized for the best performance, which is found to be 100nm. The absorption band is shifted down in wavelength as shown in Fig. 7. The absorption band is covering the range from 3.2μm to 4.2μm with only 30% of FWHM. The largest computed cell size to wavelength ratio is around 0.62λ. It is clear that the proposed absorber has improved performance in terms of cell size ratio, FWHM and absorption strength.

Table 2 lists some of the previously reported results in the IR regime compared to the results obtained in this work. The proposed absorber design possesses the smallest cell size as well as the largest bandwidth with a high absorption level.

TABLE 2
COMPARISON OF THE PROPOSED DESIGN PERFORMANCE WITH SOME PREVIOUSLY REPORTED WORK

Reference / Parameter	Guo *et al.* [15]	Shahmarvandi *et al.* [26]	Cheng *et al.* [27]	Cue *et al.* [14]	Wu *et al.* [28]	Bouchon et al. [29]	Proposed Design
Cell Size	0.85λ	0.5λ	2.1λ	0.71λ	0.7λ	0.69λ	0.34λ
FWHM	50%	35%	46%	31.3%	22%	30%	60%
Absorption Level	90%	87%	35%	85%	85%	45%	83%

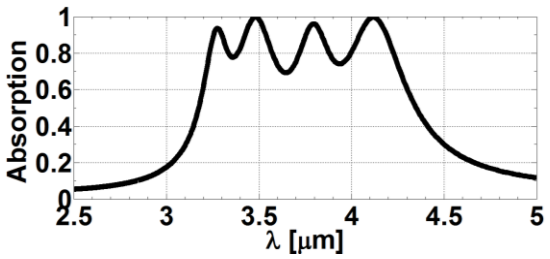

Fig. 7. Absorption response for wideband structure without nano-pillars

B. Angle Dependency Study

Further investigation is conducted by studying the angle dependence on absorption performance. The incident wave is obliquely propagating with either transvers electric (TE) or magnetic (TM) polarization. The inclination angle θ indicates the angle between the incident wave vector and the surface normal vector (*z*-axis). The azimuthal angle, Φ, represents the angle between the projection of the wave vector on the *x*-*y* plane and the *x*-axis. The graphical demonstration of these angles is illustrated in Fig. 6a. Since the discs are arranged in a hexagonal shape, i.e. each disc is surrounded by six discs, it is expected that the response should not depend on the azimuthal angle variation, Φ. It can be seen from the absorption strength versus azimuthal angle for TE polarization in Fig. 8a that the absorption strength stays strong for all angles. A similar behavior is observed for TM polarization in Fig. 8b. It is clear that the absorption level is almost independent to the variation of the azimuthal angle for both TE and TM polarizations. When the elevation angle, θ, is varied for the TE case, the absorption level is very high for angles less than 60^o as seen from Fig. 8c. A significant drop in the absorption level is noticed when the angle goes beyond $\theta=60^o$. This is due to the weakening of the tangential magnetic field component of the incident wave that maintains a strong magnetic resonance. On the other hand, the tangential magnetic field strength is fixed as the incident angle increases in the case of TM polarization. The electric field component

strength decreases; and the electric resonance weakens when the angle θ increases as seen from Fig. 8d. It is worth mentioning that the bandwidth is almost unaffected at higher incident angles. This behavior shows an enhanced performance in terms of bandwidth, absorption level and cell size to wavelength ratio compared to previous work based on multi-sized elements in the IR regime [27], [14], [30].

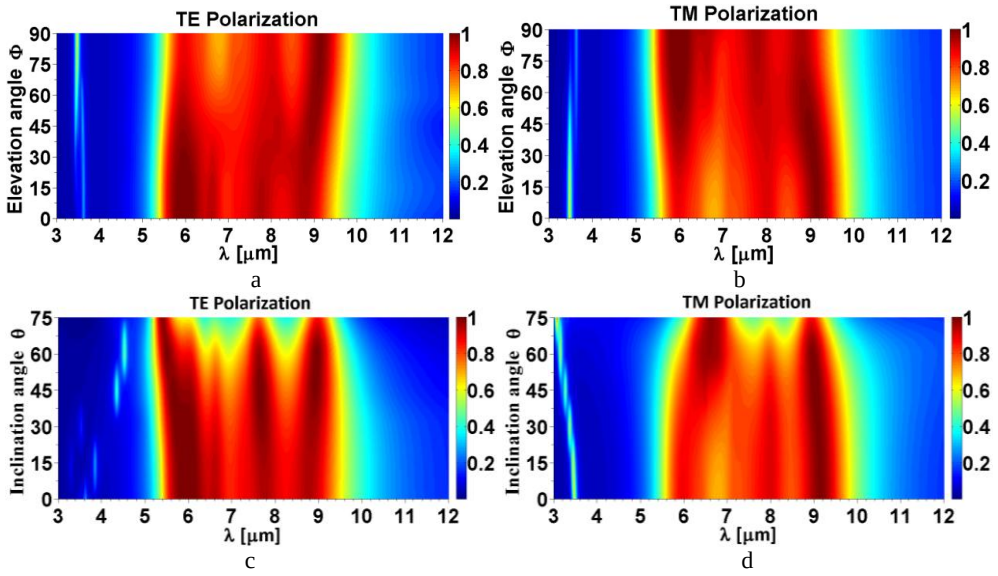

Fig. 8. Variation of incident wave azimuthal angle "Φ" for: a) TE polarization, b) TM polarization; and inclination angle "θ", c) TE polarization, d) TM polarization

C. Discs Arrangement Study

It is worth mentioning that the way the four multi-sized discs are distributed within the unit cell has a direct impact on absorption characteristics. In order to demonstrate the effect, three different arrangements are studied as shown in Fig. 9.

The first arrangement has a unit cell, where each disc is surrounded by six adjacent discs to form a hexagonal shaped arrangement as depicted in Fig. 9a. The radii of these discs are $R_1 = 0.45\mu m$, $R_2 = 0.38\mu m$, $R_3 = 0.35\mu m$, and $R_4 = 0.31\mu m$. The spacing between each two neighboring discs is varied from $0.2 - 0.5\mu m$. The absorption magnitude for TE and TM polarizations is plotted in Fig. 9a. As expected, larger spacing reduces the absorption strength, while resonances are still occurring at the same wavelengths. The second arrangement, which is depicted in Fig. 9b, has a square shaped arrangement. Each disc is surrounded by four equally spaced discs. A similar behavior is observed for the absorption response when spacing increases for both polarizations. The third arrangement is formed from a row of four equally spaced discs as shown in Fig. 9c. Due to the lack of symmetry in the structure, the absorption response for the TE polarization is completely different from the TE polarization case.

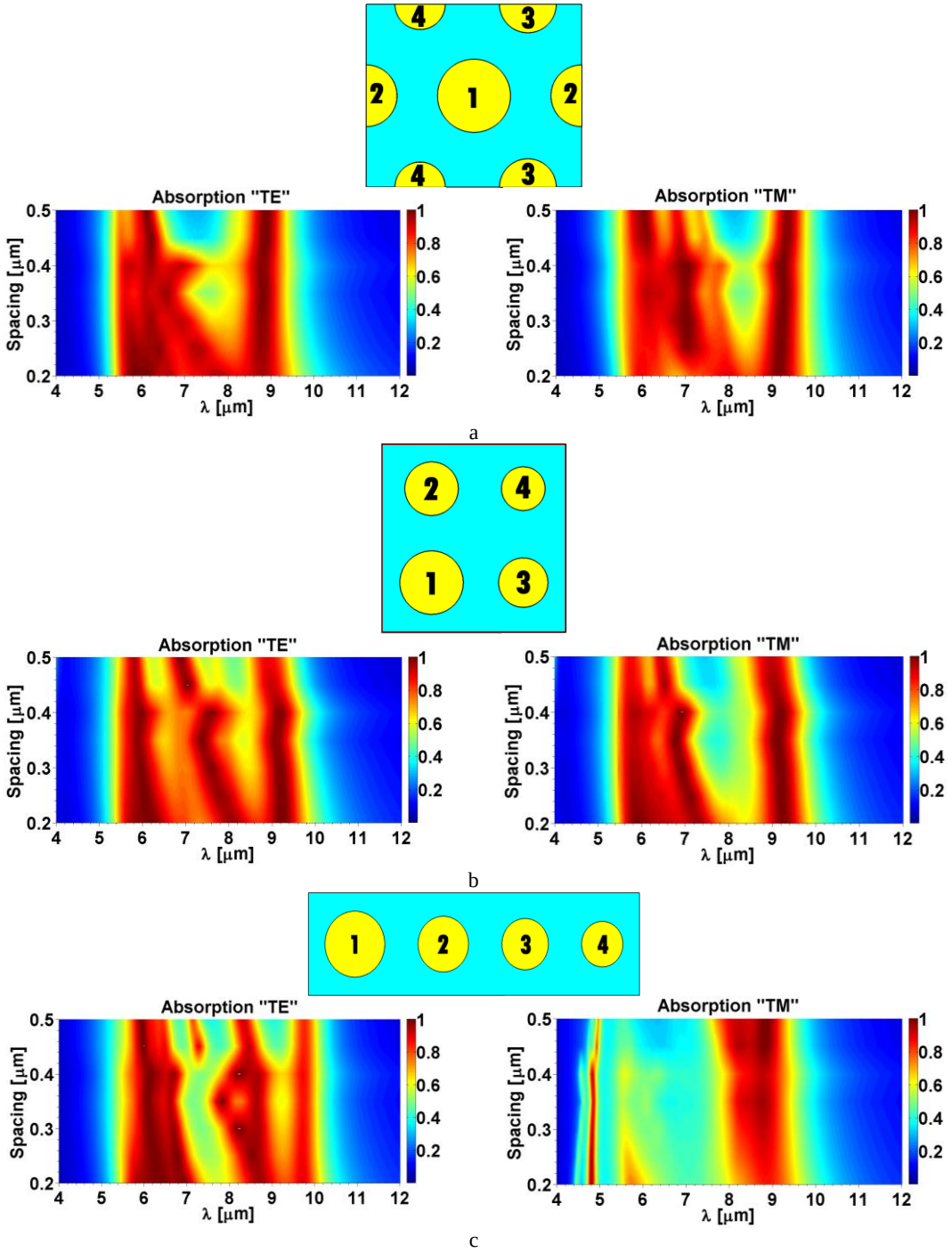

Fig. 9. Effect of spacing between adjacent discs for TE and TM polarizations: a) arrangement1, b) arrangement2, and c) arrangement3

V. CONCLUSIONS

A metamaterial based IR absorber was presented and analyzed in details. The absorber was designed to have a controllable absorption band by adjusting nano-pillar inclusions. It was shown that the resonance wavelength could be shifted up in wavelength by increasing the pillar's height. Furthermore, the bandwidth was extended using four multi-sized elements to achieve 60% FWHM with an absorption level better than 83% over the range 5.2-9.8μm. The cell size to wavelength ratio has been decreased significantly to a value of 0.34λ, which might reduce the effect of scattering at shorter wavelengths. The proposed wideband absorber possessed good absorption strength for a wide range of incident angles. The results obtained

in this work are better than many other previously reported designs that are based on the same technique in terms of cell size ratio, FWHM and average absorption level. This makes the proposed absorber suitable for diverse applications such as solar cells, light harvesting, IR spectrometers and thermal imaging applications. The work presented in this paper will develop the existing state of art of MTM based IR absorbers.

REFERENCES

[1] J. Hao, J. Wang, X. Liu, W. J. Padilla, L. Zhou, and M. Qiu, "High performance optical absorber based on a plasmonic metamaterial," *Applied Physics Letters*, vol. 96, no. 25, pp. 251104, 2010.

[2] H. Jaradat, Y. Eit-Al-Aoud, and A. Akyurtlu, "Design and characterization of metamaterial-based dual band absorber for infrared applications," *Journal of Optics*, pp. 1-6, 2016.

[3] Y. Bai, L. Zhao, D. Ju, Y. Jiang, and L. Liu, "Wide-angle, polarization independent and dual-band infrared perfect absorber based on l-shaped metamaterial," *Optics Express*, vol. 23, no. 7, pp. 68-74, 2015.

[4] P. Rufangura and C. Sabah, "Dual-band perfect metamaterial absorber for solar cell applications," *Vacuum*, vol. 120, pp. 68-74, 2015.

[5] N. Zhang, P. Zhou, L. Zhang, X. Weng, J. Xie, and L. Deng, "Ultra-broadband absorption in mid-infrared spectrum with graded permittivity metamaterial waveguide structure," *Applied Physics B*, vol. 118, no. 3, pp. 409-415, 2015.

[6] Y. Yoo, H. Zheng, Y. Kim, J. Rhee, J. Kang, K. Kim, H. Cheong, Y. Kim, and Y. Lee, "Flexible and elastic metamaterial absorber for low frequency, based on small-size unit cell," *Applied Physics Letters*, vol. 105, no. 4, pp. 041902, 2014.

[7] B. Wang, L. Wang, G. Wang, W. Huang, X. Li, and X. Zhai, "Frequency continuous tunable terahertz metamaterial absorber," *Lightwave Technology*, vol. 32, no. 6, pp. 1183-1189, 2014.

[8] H. Jaradat and A. Akyurtlu, "Infrared (IR) absorber based on multiresonant structure," *IEEE Antennas and Wireless Propagation letters*, vol. 11, pp. 1222-1225, 2012.

[9] S. Kuznetsov, A. Paulish, A. Gelfand, M. Astafiev, A. Arzhannikov, V. Fedorinin, and M. Thumm, "Extremely thin metamaterial absorbers for subterahertz waves: from fundamentals towards applications in uncooled bolometric sensors," *Proceedings of SPIE Metamaterials VII*, vol. 8423, pp. 84230S, 2012.

[10] K. Alici and E. Ozbay, "Photonic metamaterial absorber designs for infrared solar-cell applications," *Proceedings of SPIE: Next Generation (Nano) Photonic and Cell Technologies for Solar Energy Conversion*, vol. 77721, pp. 77721B, 2010.

[11] K. Chen, R. Adato, and H. Altug, "Dual-band perfect absorber for multispectral plasmon-enhanced infrared spectroscopy," *ACS NANO*, vol. 6, no. 9, pp. 7998-8006, 2012.

[12] Y. Cui, K. Fung, J. Xu, H. Ma, Y. Jin, S. He, and N. Fang, "Ultrabroadband light absorption by a sawtooth anisotropic metamaterial slab," *Nano Letters*, vol. 12, no. 3, pp. 1443-1447, 2012.

[13] X. He , Sh. Yan, Q. Ma, Q. Zhang, P. Jia, F. Wu, and J. Jiang, "Broadband and polarization-insensitive terahertz absorber based on multilayer metamaterials," *Optics Communications*, vol. 340, pp. 44-49, 2015.

[14] Y. Cui, J. Xu, K. Fung, Y. Jin, and A. Kumar, "A thin film broadband absorber based on multi-sized nanoantennas," *Applied Physics Letters*, vol. 99, no. 25, pp. 253101, 2011.

[15] W. Guo, Y. Liu, and T. Han, "Ultra-broadband infrared metasurface absorber," *Optics Express*, vol. 24, no. 18, pp. 20586-20592, 2016.

[16] W. Chen, M. Koirala, X. Liu, T. Tyler, K. West, C. Bingham, T. Starr, A. Starr, N. Jokerst, and W. Padilla, "Characterization of surface electromagnetic waves and scattering on infrared metamaterial absorbers," *E-print* http://arxiv.org/abs/1212.2868, 2012.

[17] J. Chou, Y. Yeng, A. Lenert, V. Rinnerbauer, I. Celanovic, M. Soljacic, E. Wang, and S. Kim, "Design of wide-angle selective absorbers/emitters with dielectric filled metallic photonic crystals for energy applications," *Optics Express*, vol. 22, no. S1, pp. A144-A154, 2014.

[18] H. Jaradat, "Metamaterial based infrared absorbers," *Ph.D. Dissertation*, Department of Electrical and Computer Engineering, University of Massachusetts, Lowell, MA, 2014.

[19] B. Khuyen, B. Tung, N. Dung, Y. Yoo, Y. Kim, K. Kim, V. Lam, J. Yang, and Y. Lee, "Size-efficient metamaterial absorber at low frequencies: design, fabrication, and characterization," *Journal of Applied Physics*, vol. 117, no. 24, pp.243105, 2015.

[20] N. Wang, X. Dong, W. Zhou, C. He, W. Jiang, and S. Hu, "Low-frequency metamaterial absorber with small-size unit cell based on corrugated surface," *AIP Advances*, vol. 6, no. 2, pp. 025205, 2016.

[21] A. Zayats and I. Smolyaninov, "Near-field photonics: surface plasmon polaritons and localized surface plasmons," *Journal of Optics A: Pure and Applied Optic*, vol. 5, no. 4, pp. S16-S50, 2003.

[22] N. Liu, M. Mesch, T. Weiss, M. Hentschel, and H. Giessen, "Infrared perfect absorber and its application as plasmonic sensor," *Nano Letters*, vol. 10, no. 7, pp. 2342-2348, 2010.

[23] *CST Microwave Studio 2010*, http://www.cst.com [Online].

[24] M. Ordal, R. Bel, R. Alexander, L. Long, and M. Querry, "Optical properties of fourteen metals in the infrared and far infrared: Al, Co, Cu, Au, Fe, Pb, Mo, Ni, Pd, Pt, Ag, Ti, V, and W," *Applied Optics*, vol. 24, no. 24, pp. 4493-4499, 1985.

[25] Y. Cheng, X. Mao, C. Wu, L. Wu, and R. Gong, "Infrared non-planar plasmonic perfect absorber for enhanced sensitive refractive index sensing," *Optical Materials*, vol. 53, pp. 195-200, 2016.

[26] E. Shahmarvandi, M. Ghaderi, N. Ayerden, G. Graaf and R. Wolffenbuttel, "CMOS-compatible metamaterial-based wideband mid-infrared absorber for microspectrometer applications," *Proceedings of SPIE*, vol. 9883, pp. 988309, 2016.

[27] C. Cheng, M. Abbas, C. Chiu, K. Lai, M. Shih, and Y. Chang, "Wide-angle polarization independent infrared broadband absorbers based on metallic multisized disk arrays," *Optics Express*, vol. 20, no. 9, pp.10376-10381, 2012.

[28] C. Wu and G. Shvets, "Design of metamaterial surfaces with broadband absorbance," *Optics Letters*, vol. 37, no. 3, pp. 308-310, 2012.

[29] P. Bouchon, C. Koechlin, F. Pardo, R. Haïdar, and J. Pelouard, "Wideband omnidirectional infrared absorber with a patchwork of plasmonic nanoantennas," *Optics Letters*, vol. 37, no. 6, pp. 1038-1040, 2012.

[30] X. Liu, T. Tyler, T. Starr, A. Starr, N. Jokerst, and W. Padilla, "Taming the blackbody with infrared metamaterials as selective thermal emitters," *Physical Review Letters*, vol. 107, no. 4, pp. 045901, 2011.